Journal of Asian Ceramic Societies

ISSN: (Print) 2187-0764 (Online) Journal homepage: https://www.tandfonline.com/loi/tace20

Study of physical and dielectric properties of bio-waste-derived synthetic wollastonite

Sk S. Hossain & P. K. Roy

To cite this article: Sk S. Hossain & P. K. Roy (2018) Study of physical and dielectric properties of bio-waste-derived synthetic wollastonite, Journal of Asian Ceramic Societies, 6:3, 289-298, DOI: 10.1080/21870764.2018.1508549

To link to this article: https://doi.org/10.1080/21870764.2018.1508549

Accepted author version posted online: 05 Aug 2018.
Published online: 03 Sep 2018.

JOURNAL OF ASIAN CERAMIC SOCIETIES
2018, VOL. 6, NO. 3, 289–298
https://doi.org/10.1080/21870764.2018.1508549

THE CERAMIC SOCIETY OF JAPAN
THE KOREAN CERAMIC SOCIETY
Taylor & Francis
Taylor & Francis Group

FULL LENGTH ARTICLE

Study of physical and dielectric properties of bio-waste-derived synthetic wollastonite

Sk S. Hossain and P. K. Roy

Department of Ceramic Engineering, IIT (BHU), Varanasi, India

ABSTRACT

The aim of this study is to fabricate synthetic wollastonite from chicken eggshells (CES) and rice husk ash (RHA) through an economical solid-state route. Wollastonite was formulated with a stoichiometric amount of calcined eggshells (~99% CaO) and heat-treated RHA (~93% SiO_2) as ingredients and calcined at 1000, 1100, 1150 and 1200°C for 120 min. The XRD spectrum revealed single-phase para-wollastonite (monoclinic, P21/a) after annealing at 1100°C and 1200°C with calcined powder contents comprising mainly a phase of pseudo-wollastonite (anorthic, C-1). For dielectric measurement, only the para- and pseudo-wollastonite pressed powder was sintered at 1100 and 1200°C for 240 min. The obtained results showed a stable, low dielectric constant (ε′) of about 4.5 to 6, losses (tanδ) of about 0.0026 to 0.00361 and resistivity of around 6–9 × 10^8 (Ω-cm) at 100 kHz. These are highly promising characteristics which suggest that waste-derived synthetic wollastonite may be useable as an ingredient in electrical porcelain applications.

ARTICLE HISTORY
Received 3 May 2018
Accepted 2 August 2018

KEYWORDS
Wollastonite; waste materials; eggshells; rice husk ash; dielectric properties

1. Introduction

Wollastonite is a calcium silicate mineral with the chemical formula $CaSiO_3$. According to its crystal structure, it is among the pyroxenoid group of inorganic materials containing infinite chains of [SiO_4] tetrahedral [1]. The chain motif in wollastonite is formed by two apex-to-apex combination tetrahedra, one of which is a tetrahedron with a corner parallel to the Si–O chain direction. The Si–O chains are coordinated to Ca [2]. It has a polymorphic structure, the most common triclinic or monoclinic phase is a low-temperature phase, i.e. β-$CaSiO_3$ (para wollastonite), and the other is a high-temperature phase, i.e. α-$CaSiO_3$ (pseudo wollastonite) [3]. Some properties of wollastonite, i.e. its low dielectric constant, low dielectric loss, low volatile content, high brightness, whiteness, low shrinkage, low thermal expansion, low moisture absorption, thermal stability and fluxing properties, are highly useful for industrial applications [4]. The use of wollastonite by the ceramics industry to obtain ceramics with better performance parameters is increasing rapidly, improving sales results worldwide by 30%–40%. It also offers useful applications for other industries, such as applications as a metallurgical flux for welding, as an additive in paints, as plastics to improve tensile and flexural strength, as a material for civil construction, and as a medical material for artificial bones and dental roots [5,6]. World demand for wollastonite is therefore steadily expanding.

Many researchers are consequently studying ways of fabricating synthetic wollastonite for different purposes using various raw materials and synthesis techniques. Vakalova et al. [7]derived wollastonite through mixtures of calcium carbonate with technogenic siliceous stock (micro silica, gaize or diatomite) by a solid-state method. Papynov et al. [8] synthesized porous wollastonite ceramic using a combination of sol-gel (template) and spark plasma-sintering (SPS) processes. Leite et al. [9] produced wollastonite base insulating materials using avian eggshell waste as a source of calcium oxide (CaO) and chamotte as a source of silica (SiO_2). Vichaphund et al. [10] produced wollastonite using eggshell waste through microwave synthesis. Ismail et al. [11] derived wollastonite from rice straw ash and limestone. Wu et al. [12] fabricated porous β-$CaSiO_3$ scaffolds for application in bone regeneration by a chemical precipitation method. The present work was conducted to fabricate high-purity wollastonite using 100% abandoned biowaste, i.e. eggshells and rice husk ash (RHA), by a conventional solid-state route. We also compare the characteristics of β and α-wollastonite. To the best of our knowledge, there has been no such investigation of $CaSiO_3$ ceramic materials produced with a combination of eggshell and RHA.

Egg shells are available as waste from the food-processing industry. They are disposed of in immense amounts on a daily basis causing serious pollution and public health problems. It is therefore important to recycle this waste to preserve the environment. Avian

CONTACT P. K. Roy pkroy.cer@itbhu.ac.in Department of Ceramic Engineering, IIT (BHU), Varanasi 221005, Uttar Pradesh, India

eggs contain ~11 wt.% of eggshell waste to the total weight of the egg and this waste contains around 94 wt. % $CaCO_3$, 1 wt.% $MgCO_3$, 1 wt.% $Ca_3(PO_4)_2$ and 4 wt. % organic matter [13,14]. When eggshells are calcined at above 700°C, however, all phases except CaO are removed[15]. Their chemical composition and availability have indicated them as an alternative calcium source in ceramic formulations instead of naturally occurring mineral limestone, use of which leads to conversion of natural minerals and production of waste.

Rice is considered one of the world's most important food items and is consumed by nearly half of the world's population [16]. The production of rice is growing with demand for cereal as the population increases. During the industrial processing of rice grains, about 80 wt.% is obtained as rice and approximately ~20 wt.% as by-product, i.e. rice husk (RH). This RH contains about 70–80% organic volatile matter and a remaining 20–30% mineralogical components such as silica, alkalis and trace elements [17]. It has very low nutritional value and takes a very long time to decompose. It is thus not suitable for animal feed, composting or manure. However, RH has significant calorific value (~800 kW/ton); it can be used as a fuel to generate bio-energy in boilers through direct combustion or by gasification [18]. Upon incineration, RH generates new waste in the amount of around 18–25 wt.%, namely rice husk ash (RHA), which causes environmental pollution as well as disposal problems, since only a small quantity of RHA, is used in agriculture and the brick industry. RHA is composed primarily of silica at greater than 92 wt.%; its characteristics depend on the ecological circumstances of its origin as well as the combustion conditions [19]. This silica has a large spectrum of applicability in industries, including chemicals, electronics and others [20]. Ceramic industries have also used this silica to replace quartz in applications such as ceramic pigments [21], glass-ceramics [22], refractories [23], mullite [24], cordierite [25], forsterite [26] and silicon carbide [27].

The present work was conducted to investigate the feasibility of using of waste eggshells and abandoned rice husk ash as raw materials to derive synthetic wollastonite for use as a low dielectric ingredient in ceramic bodies. Special attention is given to the preparation characteristics of the synthesized wollastonite and the dielectric properties of the sintered β and α-wollastonite. As stated above, no research has yet been done in the direction of utilization of the same for sustainable, eco-friendly wollastonite, so is unique the present work in dealing with this issue.

2. Material and methods

The present investigational study was accomplished using chicken eggshells and rice husk ash as raw materials, and the conventional solid-state route was adopted for the synthesis of wollastonite powder. The preparation flow chart for wollastonite is shown in Figure 1. Eggshells were collected from a nearby restaurant. They were cleaned in tap water and dried in sunlight. Later the shells were initially crushed using a domestic mixer, and dry milling was than conducted in a ball mill for about 4 h at 300 rpm and a weight ratio of balls to powder of about 5:1. The milled mass was then calcined at 950°C for 2 h in an air atmosphere. RHA was collected from a local rice mill where rice husks were often used as a fuel. This RHA contained a trace amount of volatile matter as well as carbon. To eliminate the carbon, the RHA was heated further at 700°C for 2 h, and ball milling was conducted for 4 h.

Wollastonite powder with the general formula CaO. SiO_2 was prepared by the solid-state reaction method using a stoichiometric (1:1 molar) amount of calcined eggshells (~99% CaO) and heat-treated RHA (~93% SiO_2) as ingredients. Two respective powders were wet ball-milled in water media for 4 h at 600 rpm. The mixture was then dried at 110°C and calcined at four different temperatures, 1000, 1100, 1150 and 1200°C, for 2 h in an air atmosphere. The agglomerate calcined particles were than dry-milled for 2 h at 600 rpm. For the pellet formation, the calcined grinding powder was granulated with 3 wt.% polyvinyl alcohol (PVA) as a binder and pressed under a uniaxial hydraulic press at a pressure of 200 MPa. The pressed plates were than sintered at the calcination temperatures (to maintain the phases well), i.e. 1100°C calcined powder was sintered at 1100°C and 1200°C calcined powder was sintered at 1200°C in an air atmosphere with a heating and cooling rate 2°C/minute and a soaking period of 4 h.

Differential thermal and thermo-gravimetric analysis (DTA–TGA) was carried out for the eggshells and RHA in an air atmosphere with a heating rate of 5°C/min using "KEP- Technologies, Setaram-Scientific & Industrial Equipment, France (Model-Labsys, Serial no-560/51,920)." The phase identification was characterized by X-ray diffraction measurements with an X'Pert Pro diffractometer using Cu-kα radiation in the range from 20° to70° with a step size of 0.02°. The crystallite size of the studied powders was evaluated using Debye–Scherrer's equation as follows:

$$t = 0.9\lambda/\beta cos\theta \quad (1)$$

where β is the full width at half-maximum (in radian) of the peaks, t is the crystallite size, θ is the Bragg diffraction peak position and λ is the wavelength of the Cu–Kαradiation (0.15405 nm). The sintering behaviors of wollastonite were investigated using thermal mechanical analysis (Netzsch DIL 402C, Germany) with a 5°C/min heating rate in air up to 1250°C. The molecular structure of the calcined powders was studied using Fourier

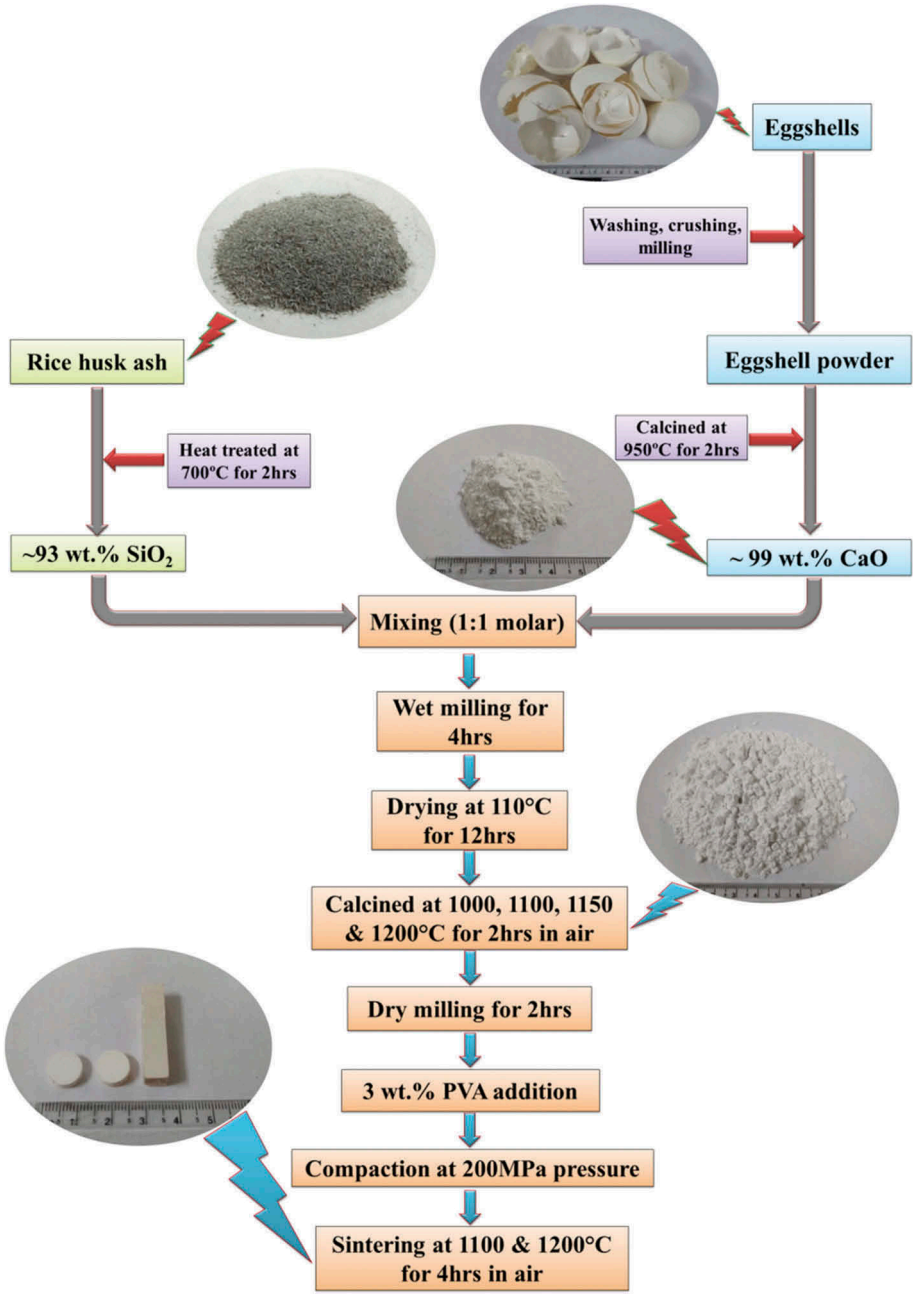

Figure 1. Flowchart of wollastonite preparation.

transform infrared spectroscopy (BRUKER, TENSOR 27-3772) between 4000 and 400 cm^{-1} by the attenuated total reflection (ATR) method to confirm the type of bonding present in the materials. The microstructure and elemental composition of the raw materials, calcined and sintered wollastonite, were observed with a scanning electron microscope (SEM) and energy-dispersive X-ray spectroscopy (EDX), respectively (Nova Nano SEM 450, FEI, Netherlands). The bulk density and porosity of the sintered samples were measured according to the Archimedes principle. The mechanical properties were determined according to the method defined in ASTM C133 by Universal Testing Machine, Tinius Olsen, H10KL-I0129 [28]. High-purity silver electrode paste was coated on both surfaces of sintered wollastonite pellets and cured at 150°C for 2 h for dielectric property measurements using an impedance analyzer (Key Sight Technology, Model-E4990A). The dielectric constant (ε') and AC resistivity (ρ) were evaluated by the flowing formula as follows:

$$\varepsilon' = cd/A\varepsilon_o \tag{2}$$

$$\rho = 1/(\omega\varepsilon_o\varepsilon' tan\delta) \tag{3}$$

respectively, where, c is the capacitance, d is the sample thickness, A is the sample area, ε_o is the permittivity of free space (8.85×10^{-12} F/m), ω is the angular frequency ($2\pi f$), f is the linear frequency and $tan\delta$ is the dissipation factor.

3. Results and discussion

3.1. Characterization of raw materials

Figure 2(a) shows the thermal behavior analysis of dry eggshell powder up to 1000°C. A slight weight loss of around 5wt.% is observed in the TGA curve in the temperature range from 100°C to 700°C due to the removal of combined water and organic compounds (rich in protein fibers) present in the eggshells. An exothermic event is observed at around 200 to 550°C in the DTA curve, probably due to the burning of organic matter from the shell membrane. The wide weight loss occurring at about 850°C is due to the decomposition of $CaCO_3$, which is attributed to an endothermic peak in the DTA curve. The total loss of eggshell is around 44 wt.%. Eggshells are composed primarily of calcite ($CaCO_3$), and calcined eggshell powder is composed mainly of portlandite [$Ca(OH)_2$], which is confirmed by the XRD studies shown in Figure 3(a,b), respectively. The portlandite is probably formed by absorption of moisture from the atmosphere by calcium oxide (CaO). A similar phenomenon was observed by Leite et al. [9]. Table 1 represents the chemical composition of calcined eggshells; it is found that the powder contains greater than 99% of CaO. Figure 4(a) exhibits the particle morphology of the calcined eggshell powder. The particles are uneven in shape, and the average size is 0.50μm, as estimated from the SEM micrograph using "Image J1.48V" software.

The DTA–TGA curve for the pulverized rice husks up to 1000°C is shown in Figure 2(b). In the TGA curve, the small weight loss detected up to 200°C may be due to evaporation of physical water. The large exothermic peak at 400°C (shown in the DTA curve) is due to the burning of organic matter, which also contributed to the enormous weight loss. About ~77 wt. % of the total weight of RH is removed when the temperature rises to 480°C, and the weight then remains unchanged up to 1000°C. Figure 3(c) shows the XRD curve of heat-treated RHA. The absence of any sharp peak demonstrates that the silica in the RHA is in amorphous form only. The heat-

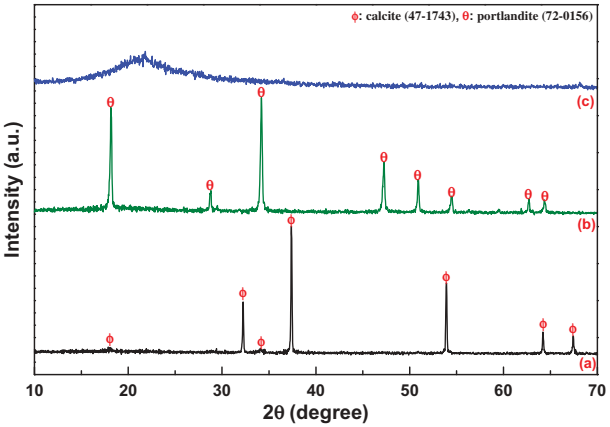

Figure 3. XRD curve of (a) eggshells, (b) calcined eggshells at 950°C and (c) heat-treated RHA at 700°C.

Table 1. The chemical composition of calcined eggshells and heat-treated RHA.

Compound (wt.%)	Calcined eggshells	RHA
SiO_2	–	93.20
Na_2O	0.17	2.86
P_2O_5	0.23	1.18
K_2O	–	1.12
CaO	99.08	0.52
Fe_2O_3	0.08	0.35
TiO_2	–	0.31
MgO	0.29	0.27
SrO	0.15	–
RuO_2	–	0.19

treated RHA contains greater than 93% of SiO_2, as shown in Table 1. Figure 4(b) shows SEM and EDX images of the heat-treated RHA. The powder is composed mainly of irregular-shaped particles with an average particle size of 1.20μm. EDX analyses were also performed to determine the elemental composition of powder, detecting only O, Si for RHA and O, Ca elements for calcined eggshells within the limits of instrument accuracy.

3.2. Characterization of calcined wollastonite

Powder XRD studies were performed at room temperature for calcined wollastonite powders after

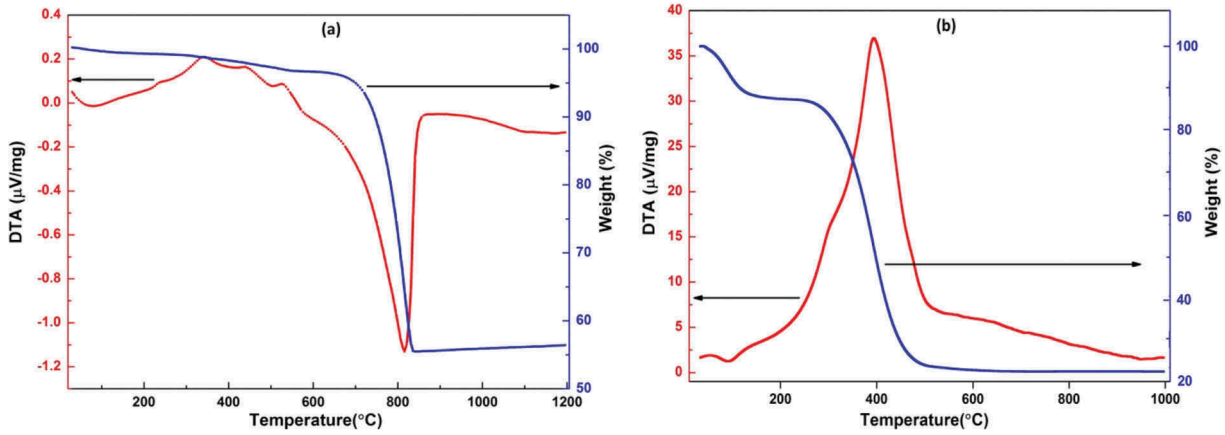

Figure 2. DTA–TGA curve of (a) eggshells and (b) rice husk.

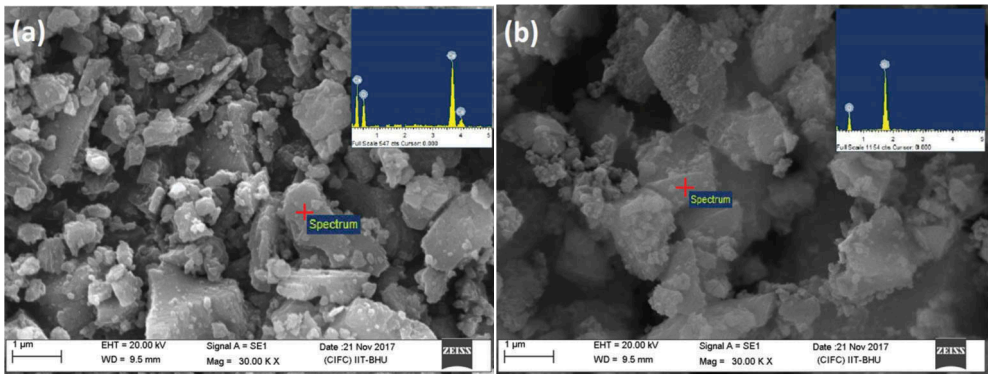

Figure 4. SEM image of (a) calcined eggshells and (b) heat-treated RHA.

milling. Figure 5 shows the XRD patterns of calcined powders heated at 1000, 1100, 1150 and 1200°C. The formation of perovskite structures of β and α-wollastonite at different calcining temperatures have been confirmed. It can be seen that the peaks of β-wollastonite, small quantity larnite (Ca_2SiO_4) and unreacted cristobalite (SiO_2) are observed at 1000°C, matching those of JCPDS file Nos 43-1460, 33-0302 and 82-0512, respectively, and that the peak of CaO disappeared [3]. The formation of the pure wollastonite phase at low temperature is greatly affected by the finesse of the ingredients [29]. It may be that highly active amorphous RHA silica and fine raw materials accelerate the diffusion reaction for the phase formation of wollastonite. Single-phase β-wollastonite (monoclinic, space group number and name-14, P21/a) is attained after calcination at 1100°C; and larnite and cristobalite are eliminated through reaction with each other. Additionally, the β-wollastonite, i.e. para wollastonite phase, is transformed to its polymorphic form of α-wollastonite, i.e. pseudo wollastonite, at high temperature [30]. At 1150°C calcined powder is composed of collaborative α and β-wollastonite phases, and at 1200°C the powder comprises mainly the pseudo wollastonite phase (anorthic, C-1) [3,10]. The crystallite sizes of the β and α-wollastonite are projected from the X-ray peak broadening of the (320) and (132) peaks of 1100 and 1200°C calcined powders, respectively. The crystallite sizes increase with the transformation of β to α-wollastonite, to 62 and 83nm, respectively. This effect occurs due to the formation of the pseudo-hexagonal structure of α-$CaSiO_3$, which contains three silicon-oxygen tetrahedra and forms a ring of $Ca_3Si_3O_9$ [31].

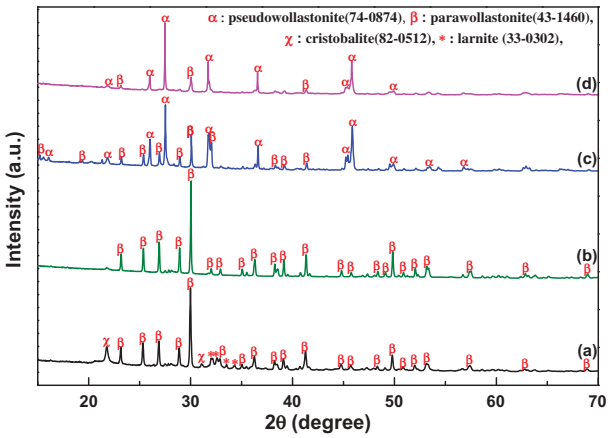

Figure 5. XRD analysis of calcined powders at (a) 1000, (b) 1100, (c) 1150 and (d) 1200°C.

In order to study the purity and formation of the chemical bonds during calcination at 1100 and 1200°C, FTIR analysis (shown in Figure 6) was performed. The formation of crystalline $CaSiO_3$ is recognized by the FTIR peaks at 432, 622 and 985 cm^{-1} [32]. A group of absorption bands in the region of 1000–1200 cm^{-1} representes asymmetric stretching vibration oscillations of the bridge bonds Si–O–Si in the [SiO_4]-tetrahedra. Strong absorption bands in the region of the spectrum at about 980–650 cm^{-1} is attributed to symmetrical stretching vibrations of the bridge and non-bridge Si–O bands [33,34]. The bonds between the 600–450 cm^{-1} spectra are assigned to the bending vibrations of the bridge and non-bridge Si–O groups [35], and the existence of Ca–O bonds in the structure, i.e.[CaO_6]-octahedra is confirmed by the peaks at 423–450 and 940 [36]. The broad band at around 890 cm^{-1} is assigned to the characteristic peaks of Si–O–Ca [37]. These peaks verify the formation of wollastonite, as they are also shown in the XRD patterns of the powder calcined at 1100°C and above.

Figure 7 shows SEM micrographs of powder calcined at 1100 and 1200°C for 2 h without grinding. The SEM results indicate that both powders are composed mainly of irregular agglomerate-shaped particles. There is a slight difference in the sizes of the wollastonite powders calcined at 1100 and 1200°C. It can be clearly observed that the average particle size is improved with increases in the calcined temperature due to the stacking together of fine wollastonite particles at high temperature to form agglomerates [9]. The average particle sizes are 2.10 and 3.60μm for calcination at1100 and 1200°C, respectively. It is also seen in the morphology that the texture of the

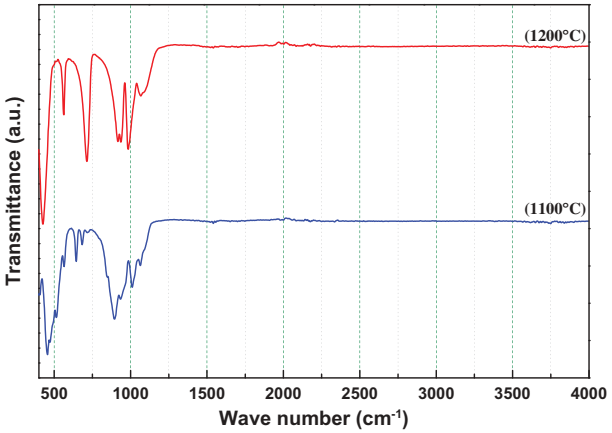

Figure 6. FTIR spectroscopy of wollastonite powders calcined at 1100 and 1200°C.

particles becomes rougher with increases in the calcination temperature. EDX analysis of the calcined powder reveals that the quantitative existence of Ca, Si and O elements in approximately their respective proportions suggests the high purity of the wollastonite powder.

3.3. Characterization of sintered wollastonite

Figure 8 demonstrates the thermal densification curve of waste-derived wollastonite powder, which was already calcined at 1200°C. No significant expansion or shrinkage behavior is observed, therefore up to 900°C. The graph shows, however that the compacted powders begin to densify at around 920°C and that the rate of the shrinkage increases with increases in temperature. Closely similar sintering behavior is observed for wollastonite in the previous studies [38,39]. The linear shrinkage values of wollastonite are 0.82, 3.9 and 6.27% for 1100, 1200 and 1250°C, respectively. These increases in the shrinkage values may be attributed to vitrification of the powder.

SEM micrographs of the wollastonite surfaces sintered at 1100 and 1200°C are presented in Figure 9. The sintered specimen at 1100°C exhibits an interconnected porous structure. A large number of open pores with different shapes is detected. The grains are uneven in shape with sizes from 0.236 to 0.487μm. An increase in the sintering temperature to 1200°C results in a dense structure with diffusion of the small grains, which enhances the size of the isometric grains of the crystalline phase and decreases the pore sizes. Vichaphund et al. [10] have reported the same characteristics for sintered wollastonite. The values for average grain size, apparent porosity, and bulk density are shown in Table 2. The porosity volume shrinks with increases in the sintering temperature, i.e. 23.37%–4.65%. A second reasons may be the formation of α-$CaSiO_3$ crystalline phases with a pseudo-hexagonal structure in the system. Si–O tetrahedra in the pseudo-wollastonite are therefore compacted further by the form of the ring structure. As a result, the surface energy of the ring is increased,

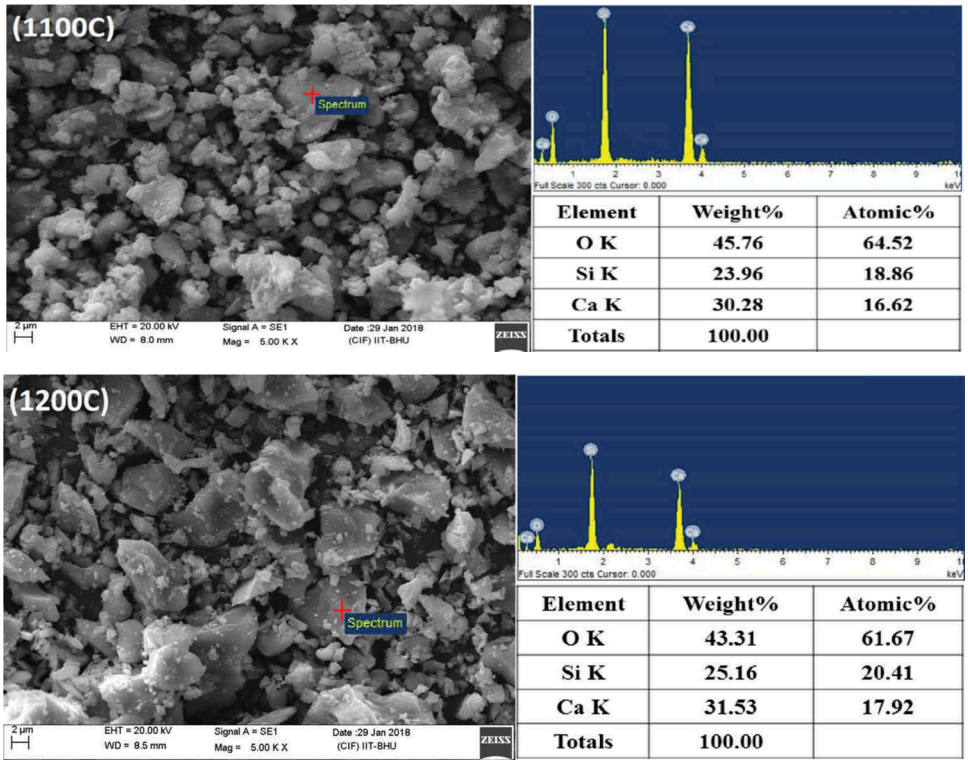

Figure 7. SEM & EDX analysis of wollastonite powders calcined at 1100 and 1200°C.

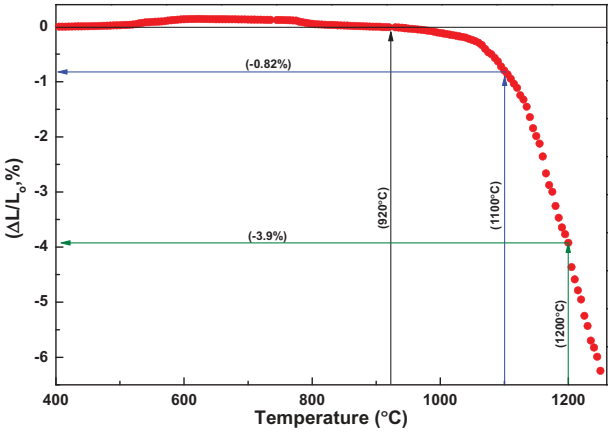

Figure 8. Shrinkage curve of wollastonite powder calcined at 1200°C and heated in air up to 1250°C.

which could be reduced by introducing a large number of atoms to increase the volume of the ring and form a compact structure by reorientation of the atoms [40].

The mean values for flexural strength at room temperature of sintered wollastonite specimens are given in Table 2. The flexural strength is significantly improved with increase in the densification temperature. This may be attributed to the decrease in porosity and pore size and the increase in the degree of sintering, as shown in the SEM micrograph and densification curve (Figures 8 and 9). Porosity in the non-ductile body accelerates the rate of crack propagation, resulting in generation of a small amount of stress toward the breakage of the structure [41].

The room temperature frequency dependency of the dielectric constant (ε′), loss angle tangent (tanδ) and AC resistivity (ρ) of the wollastonite sintered at 1100 and 1200°C are measured in the frequency range of 20 Hz to 10 MHz, as displayed in Figure 10(a–c), respectively. The values of the above-mentioned electrical properties at 100kHz are tabulated in Table 3. Both samples, i.e. 1100 and 1200°C sintered wollastonite, exhibit a low and stable dielectric constant up to a frequency of 1MHz. This may be due to the low dielectric polarizability of Si

Table 2. Apparent porosity, bulk density, grain size and flexural strength of sintered samples.

	Apparent porosity (%)		Bulk density (gm/cc)		Grain size (μm)		Flexural strength (MPa)	
Samples	Mean	s.d.	Mean	s.d.	Mean	s.d.	Mean	s.d.
1100°C	22.37	1.18	2.065	0.081	0.378	0.027	26.42	2.72
1200°C	4.65	0.87	2.603	0.046	1.235	0.013	68.85	1.63

and Ca strongly bonded in the [SiO_4]-tetrahedral and [CaO_6]-octahedra structural units of the $CaSiO_3$ resulting in polarization dominated by the hopping mechanism. Wollastonite exhibits a slight enhancement in the dielectric constant, however, with increases in the sintering temperature from 1100 to 1200°C. This may be due to increases in the density of the sample with a lower porosity and uniform microstructure [42]. Another reason may be temp oxygen vacancy increases due to the increases in the space charge polarization, resulting from dielectric constant increases. The tangent of loss (tanδ) is represents the portion of the electric field energy dissipated to heat in the ceramic body by various physical relaxation processes. It can be observed in Figure 10(b) that tanδ is very low for both samples, only 0.0029 at 100 kHz. It is also seen that the dielectric loss is nearly independent of frequency up to 1 MHz. For this reasons, wollastonite is called a "low loss ceramic" [4]. This low tanδ can be attributed to the high electrical resistivity of ~10^{10} Ω-cm at 1 kHz. A slight decrease in ρ with increases in frequency is observed in Figure 10(c), moreover, due to the inverse relationship between them. It is important, however, to maintain low-stable ε′ and tanδ in a relatively wide frequency range for the practical use of wollastonite as an ingredient for low-frequency applications in electrical porcelain bodies.

The changes in the dielectric constant and loss as a function of temperature for sintered samples at 1 MHz are presented in Figure 11(a,b), respectively. It is clear from Figure 11 that ε′ and tanδ are approximately constant from 30 to 480°C at 1 MHz for both samples. These results suggest that the temperature

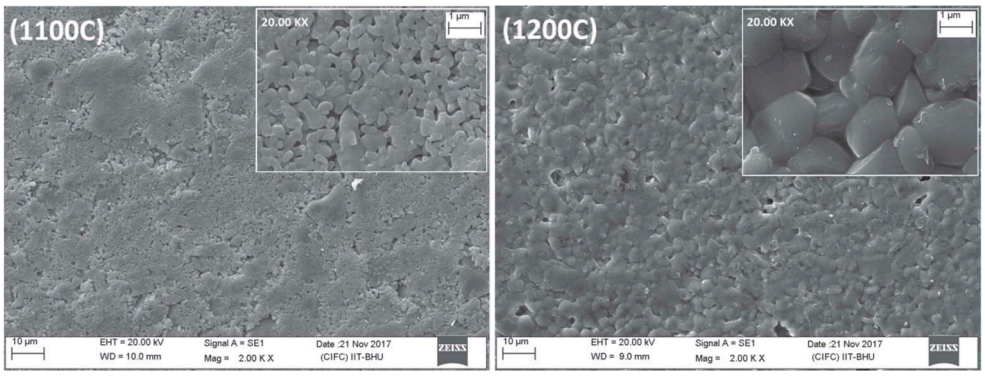

Figure 9. SEM micrograph of wollastonite sintered at 1100 and 1200°C.

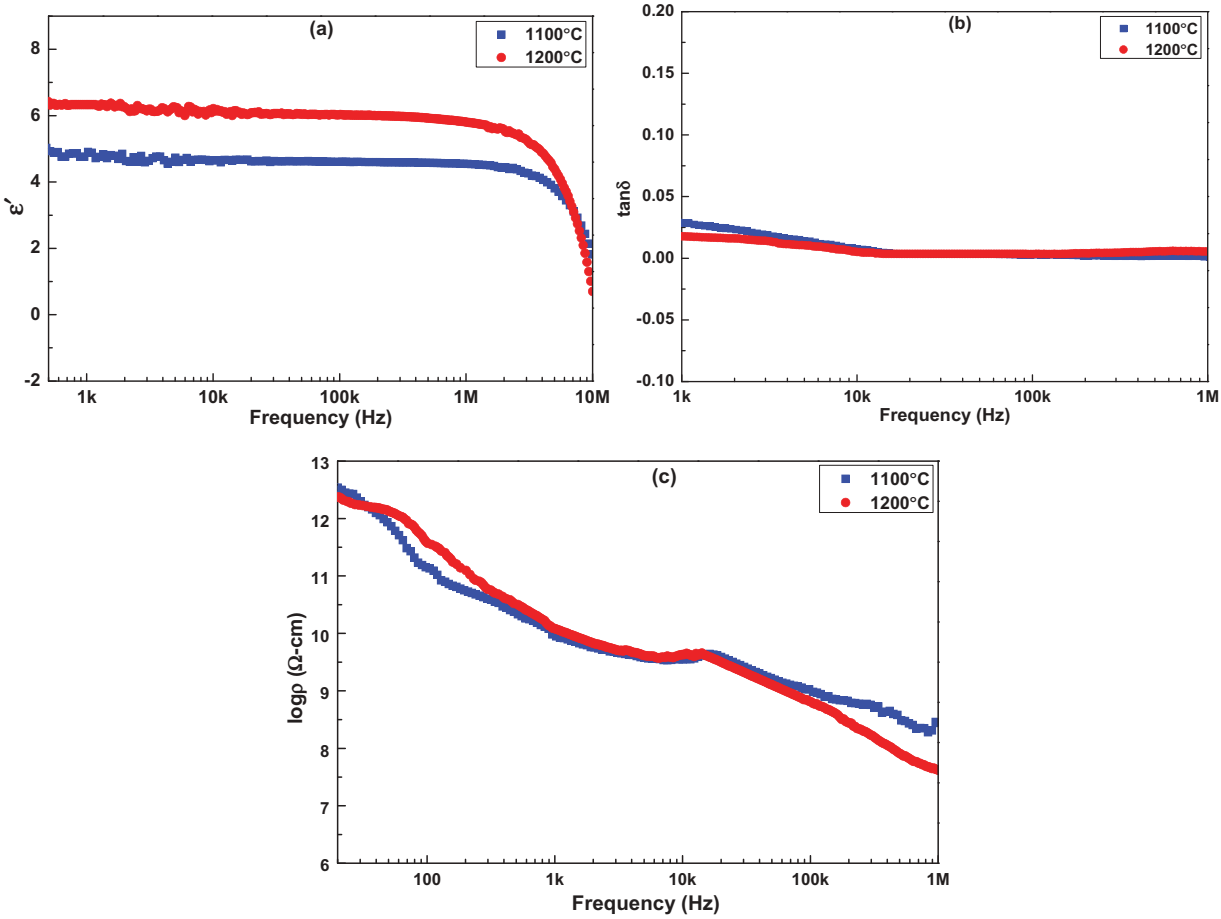

Figure 10. Changes in the (a) dielectric constant, (b) loss angle tangent (tanδ) and (c) electrical resistivity with frequency for samples sintered at 1100 and 1200°C.

Table 3. Dielectric constant, loss angle tangent and resistivity of sintered samples.

Samples	Dielectric constant (ε')$_{100kHz}$	Loss angle tangent $(\tan\delta)_{100kHz}$	Resistivity(ρ)$_{100kHz}$ (Ω-cm)
1100°C	4.62	0.00260	9.60×10^8
1200°C	6.02	0.00361	6.42×10^8

does not alter the dielectric polarization mechanisms of wollastonite up to 480°C, which may be due to the presence of strong ionic bonds in the $CaSiO_3$. Other observed effects may be due to the extremely high purity of waste-derived wollastonite.

4. Conclusions

The results of this study demonstrate that chicken eggshells and RHA can be used for the production of sustainable, high-purity synthetic wollastonite as an ingredient for ceramics and other industrial products. The physical and dielectric properties of

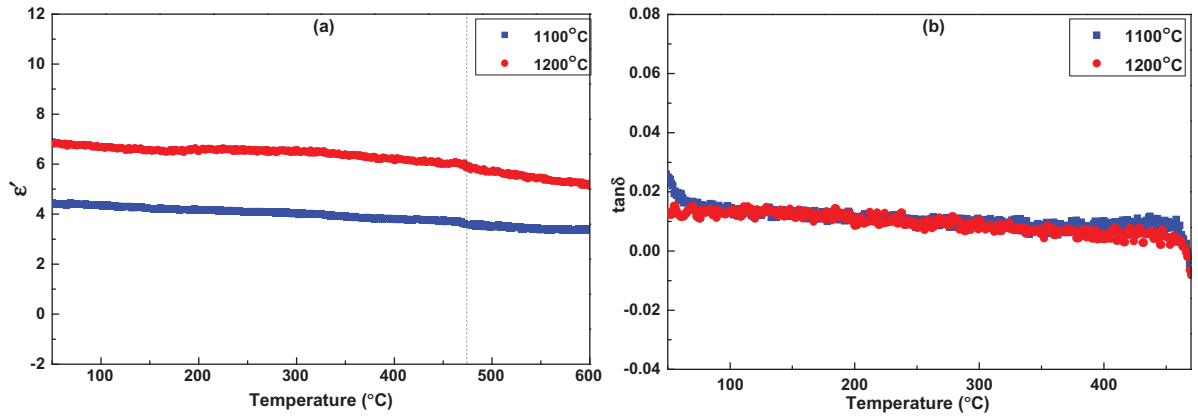

Figure 11. Changes in the (a) dielectric constant and (b) loss angle tangent (tanδ) with the temperature for samples sintered at 1100 and 1200°C.

wollastonite were investigated and the following results were obtained:

- It was found that the peak of β-wollastonite, a small quantity of larnite (Ca_2SiO_4) and unreacted cristobalite (SiO_2) are detected at 1000°C and that only β-wollastonite is observed after calcination at 1100°C.
- Powder calcined at 1150 and 1200°C contains mainly α-wollastonite and a slight portion of unconverted β-wollastonite.
- The average particle and grain sizes increase with increases in the calcined and densification temperatures of wollastonite.
- The density and mechanical strength are also improved with increases in the sintering temperature.
- The dielectric properties of wollastonite are not affected significantly, however, by the transformation of β to the α phase.
- The wide range of temperatures (30–480°C) does not alter the dielectric behavior of wollastonite.

This recycling of wastes for wollastonite formation can lead to economical and sustainable ceramics production by putting it to practical use in the electrical porcelain industry.

Acknowledgments

The authors gratefully acknowledge all the faculty and staff of the Department of Ceramic Engineering, Indian Institute of Technology (BHU), Varanasi, India, and the Ministry of Human Resource Development (MHRD), Govt. of India, for providing appreciable support.

Disclosure statement

No potential conflict of interest was reported by the authors.

ORCID

Sk S. Hossain http://orcid.org/0000-0001-7910-4993
P. K. Roy http://orcid.org/0000-0001-9854-066X

References

[1] Deer, Howie, Zussman. Rock forming minerals; single chain silicates. Vol. 2A. Second ed. London: TheGeological Society; 1997.
[2] Ohashi Y. Polysynthetuically-twinned structures of enstatiteandwollastonite. Phys Chem Miner. 1984;10 (5):217–229.
[3] Florian P, Fayon F, Massiot D. ^{2}J Si-O-Si Scalar Spin-Spin coupling in the solid state: crystalline and glassy wollastonite $CaSiO_3$. J Phys Chem C. 2009;113:2562–2572.
[4] Sen S. Ceramic whitewares: their technologies and applications. 1st ed. Vol. 169. New Delhi, India: Oxford & IBH publishing co. pvt. Ltd; 1992.
[5] Virta RL. Wollastonite, U.S. Geological Survey, Minerals Yearbook. 2009. (http://minerals.usgs.gov/minerals/pubs/commodity/wollastonite/myb1-2009-wolla.pdf)
[6] Liu XY, Ding CX, Chu PK. Mechanism of apatite formation onwollastonite coatings in simulated body fluids. Biomaterials. 2004;25:2007–2012.
[7] Vakalova TV, Pogrebenkov VM, Karionova NP. Solid-phase synthesis of wollastonite in natural and technogenic siliceous stock mixtures with varying levels of calcium carbonate component. Ceramics Int. 2016;42:16453–16462.
[8] Papynov EK, Shichalin OO, Mayorov VY, et al. Sol-gel and SPS combined synthesis of highly porous wollastonite ceramic materials with immobilized Au-NPs. Ceramics Int. 2017;43:8509–8516.
[9] Leite FHG, Almeida TF, Faria-Jr RT, et al. Synthesis and characterization of calcium silicate insulating material using avian eggshell waste. Ceramics Int. 2017;43:4674–4679.
[10] Vichaphund S, Kitiwan M, Atong D, et al. Microwave synthesis of wollastonite powder from eggshells. J Eur Ceram Soc. 2011;31:2435–2440.
[11] Ismail H, Shamsudin R, Hamid MAA, et al. Characteristics of β-wollastonite derived from rice straw ash and limestone. J Aust Ceramic Soc. 2016;52(2):163–174.
[12] Wu C, Fan W, Zhou Y, et al. 3D-printing of highly uniform $CaSiO_3$ ceramic scaffolds: preparation, characterization and in vivo osteogenesis. J Mater Chem. 2012;22:12288–12295.
[13] Tsai WT, Yang JM, Lai CW, et al. Characterization and adsorption properties of eggshells and eggshell membranes. BioresourTechnol. 2006;97:488–493.
[14] Naga SM, El-Maghraby HH, Sabed M, et al. Highly porous scaffolds made of nanosized hydroxyapatite powder synthesized from eggshell. J Ceram Sci Technol. 2015;6:237–244.
[15] Witoon T. Characterization of calcium oxide derived from waste eggshell and its application as CO_2 sorbent. Ceram Int. 2011;37(8):3291–3298.
[16] Bhullar N, Gruissem W. Nutritional enhancement of rice for human health: the contribution of biotechnology. Biotechnol Adv. 2013;31:50–55.
[17] Sarangi M, Bhattacharyya S, Behera RC. Effect of temperature on morphology and phase transformations of nano crystalline silica obtained from rice husk. Phase Transitions. 2009;82(5):377–386.
[18]. Zafar S. Rice straw as bionery resource. Bio Energy Consult. 2015;26. Available form: http://www.bioenergyconsult.com/tag/rice-straw
[19] Gonzalve MRF, Bergmann CP. Thermal insulators made with rice husk ashes: production and correlation between properties and microstructure. Constr Build Mater. 2007;12(21):2059–2065.
[20] Folleto EL, Hoffmann R, Hoffmann RS, et al. Applicability of rice husk ash. Quím Nova. 2005;28:1055–1060.
[21] Bondioli F, Andreola F, Barbieri L, et al. Effect of rice husk ash (RHA) in the synthesis of $(Pr,Zr)SiO_4$ ceramic pigment. J Eur Ceram Soc. 2007;27:3483–3488.
[22] Andreola F, Martın MI, Ferrari AM, et al. Technological properties of glass-ceramic tiles obtained using rice husk ash as silica precursor. Ceramics Int. 2013;39:5427–5435.
[23] Stochero NP, Marangon E, Nunes AS, et al. Development of refractory ceramics from residual silica derived from rice husk ash and steel fibres. Ceramics Int. 2017;43:13875–13880.

[24] Sembiring S, Simanjuntak W, Manurung P, et al. Synthesis and characterization of gel-derived mullite precursors from rice husk silica. Ceram Int. 2014;40 (5):7067–7072.
[25] Sembiring S, Simanjuntak W, Situmeang R, et al. Preparation of refractory cordierite using amorphous rice husk silica for thermal insulation purposes. Ceramics Int. 2016;42:8431–8437.
[26] Mathur L, Hossain SS, Majhi MR, et al. Synthesis of nano-crystalline forsterite (Mg_2SiO_4) powder from biomass rice husk silica by solid-state route. Bol Soc Esp Cerám Vidr. 2018;57:112–118.
[27] Singh SK, Mohanty BC, Basu S. Synthesis of SiC from rice husk in a plasma reactor. Bull Mater Sci. 2002;25 (6):561–563.
[28] ASTM C133.Standard test methods for cold crushing strength and modulus of rupture of refractories. ASTM International; 2015.
[29] Yazdani A, Rezaie HR, Ghassai H, et al. The effect of processing parameters on the hydrothermal synthesis of wollastonite at low pressure. J Ceramic Process Res. 2013;14(1):12–16.
[30] Nour WMN, Mostafa AA, Ibrahim DM. Recycled wastes as precursor for synthesizing wollastonite. Ceramics Int. 2008;34:101–105.
[31] Xia W, Chang J. Preparation and the phase transformation behavior of amorphous mesoporous calcium silicate. Micropor Mesopore Mat. 2008;108:345–351.
[32] Beaudoin JJ, Dramé H, Raki L, et al. Formation and characterization of calcium silicate hydrate–hexadecyltrimethylammonium nanostructure. J Mater Res. 2008;23(10):2804–2815.
[33] Shamsudin R, Azam FAA, Hamid MAA, et al. Bioactivity and cell compatibility of β-Wollastonite derived from rice husk ash and limestone. Materials. 2017;10:1188.
[34] Eniu D, Gruian C, Vanea E, et al. FTIR and EPR spectroscopic investigation of calcium-silicate glasses with iron and dysprosium. J Mol Struct. 2015;1084:23–27.
[35] Paluszkiewicz C, Blaz˙ewicz M, Podporska J, et al. Nucleation of hydroxyapatite layer on wollastonite material surface: FTIR studies. Vib Spectrosc. 2008;48:263–268.
[36] Sharafabadi AK, Abdellahi M, Kazemi A, et al. A novel and economical route for synthesizing akermanite($Ca_2MgSi_2O_7$) nano-bioceramic. Mater Sci Eng C. 2017;71:1072–1078.
[37] Puntharod R, Sankram C, Chantaramee N, et al. Synthesis and characterization of wollastonite from egg shell and diatomite by the hydrothermal method. J Ceramic Process Res. 2013;14(2):198–201.
[38] Karamanov A, Pelino M. Induced crystallization porosity and properties of sinteredsdiopside and wollastonite glass-ceramics. J Eur Ceram Soc. 2008;28:555–562.
[39] Cannillo V, Pierli F, Sampath S, et al. Thermal and physical characterisation of apatite/wollastonite bioactive glass–ceramics. J Eur Ceram Soc. 2009;29:611–619.
[40] Tangboriboon N, Khongnakhon T, Kittikul S, et al. An innovative $CaSiO_3$ dielectric material from eggshells by sol–gel process. J Sol-Gel SciTechnol. 2011;58:33–41.
[41] Kazmi SMS, Abbas S, Saleem MA, et al. Manufacturing of sustainable clay bricks: utilization of waste sugarcane bagasse and rice husk ashes. Constr Build Mater. 2016;120:29–41.
[42] Hu W, Liun H, Hao H, et al. Influence of TiO2 additive on the micro wave dielectric properties of α-$CaSiO_3$–al_2O_3 ceramics. Ceramics Int. 2015;41:S510–S514.